Supplemental Materials for

Mechanical response of mesoscopic aluminum rings under uniaxial compression

Bin Zhang, Shahrior Ahmed, Shuai Shao, W.J. Meng

Mechanical & Industrial Engineering Department

Louisiana State University, Baton Rouge, LA 70803

S1. Aluminum micro pillar fabrication

Commercial Al 1100 alloy (Al 99.9 at.%+) cylindrical rods, 3 mm in diameter, were annealed under vacuum (~10^{-7} Torr) at 400 °C for 1 hr. The Al rods were first mechanically polished, followed by a final vibratory polish with 50 nm silica suspension for 12 hr for electron backscatter diffraction (EBSD) examination. Figure S1(a) shows the EBSD orientation map of a typical as-annealed Al rod specimen. The average grain size was measured by the linear interception method to be ~ 30 μm, obtained from the average of grain intercepts to 78 lines automatically generated by the EBSD software.

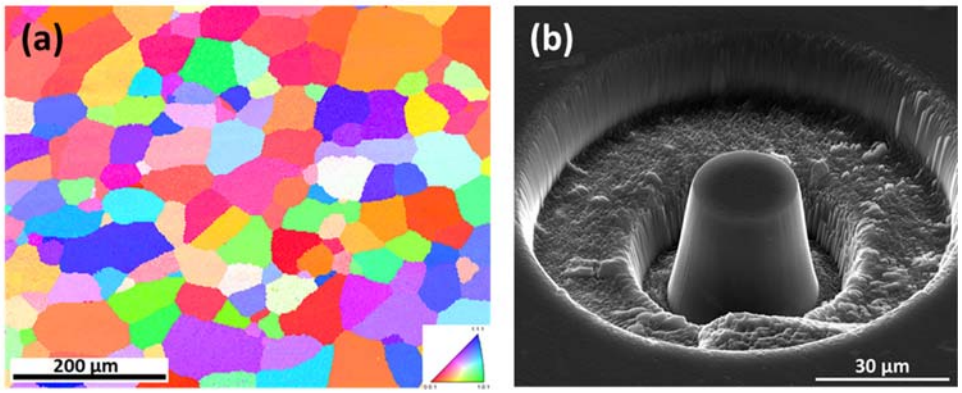

Fig. S1. (a) A typical EBSD orientation map of an as-annealed Al rod specimen. The measured average Al grain size is ~30 μm; (b) an SEM image of one typical PFIB Al pillar with a top surface diameter of 24 μm. The image was taken at a 45° tilt.

Al micro-pillars were fabricated from as annealed Al rods by Xe^+ plasma focused ion-beam (PFIB) milling in a Tescan FERA-3 Model GMH Focused Ion Beam Microscope system operated at 30 kV ion beam voltage. Pillar milling was conducted through a series of concentric top-down annular pattern millings with the Xe^+ ion current varied from 100 nA for the initial coarse milling to 10 nA for the final fine milling. The diameters of fabricated micro-pillar were ~20, ~40, and ~60 μm, with height-to-diameter ratios ranging from 1:1 to 1.5:1. The top-down milling led to the existence of a pillar taper angle, which was measured in the SEM to be ~9°. Figure S1(b) shows one typical Al pillar fabricated with PFIB, with a top surface diameter of 24 μm and a height of 33 μm. Similar pillar morphologies were observed at other pillar diameters.

S2. Uniaxial compression of Al micro-pillars

Uniaxial compression on Al pillars was carried out on a Nanoindenter XP System (MTS Systems Corp., Knoxville, TN) with nominal load and displacement resolutions of 50 nN and 0.01 nm, respectively. A flat-ended cylindrical diamond punch with a diameter of ~76 μm was used. All Al micro-pillars were compressed under the displacement-controlled mode. For pillars of different heights, the displacement rate was varied to achieve a constant engineering strain rate of 2.5×10^{-4} s^{-1}. The diamond punch – pillar alignment was achieved with the help of an optical microscope attached to the XP system and a tilt-adjustable specimen stage. In separate experiments, the flat-ended diamond punch was indented directly onto the flat part of an Al specimen surface to measure the system compliance. This measured compliance, as shown in Fig. S2, was subtracted from the measured force-displacement curves obtained from Al micro-pillars.

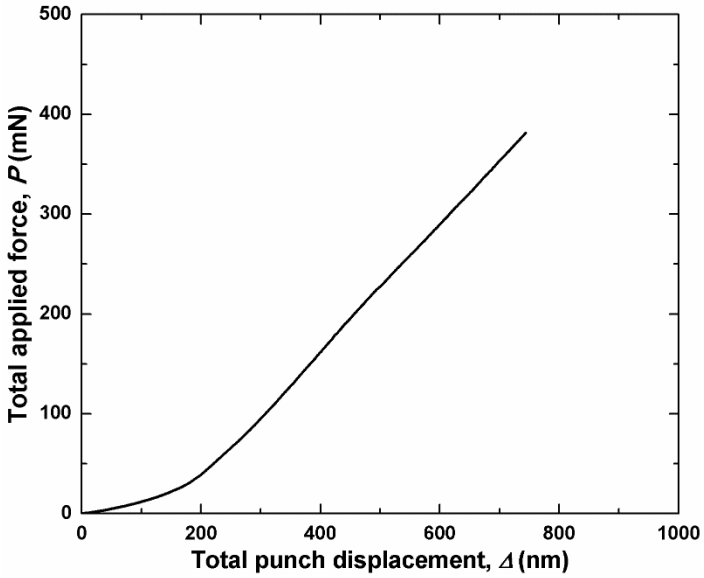

Fig. S2. System compliance measurement

Because of the existence of a taper angle on PFIB fabricated Al pillars, it is difficult to calculate the true strain from raw pillar compression force – displacement curves. The engineering strains were therefore calculated based on the initial pillars heights, as measured from the SEM images. Pillar compression stresses were calculated based on the top cross-sectional area of the pillar before testing and on the already obtained engineering strain. Figure S3 shows the so-obtained compression stress – engineering strain curves for Al micro-pillars of various diameters.

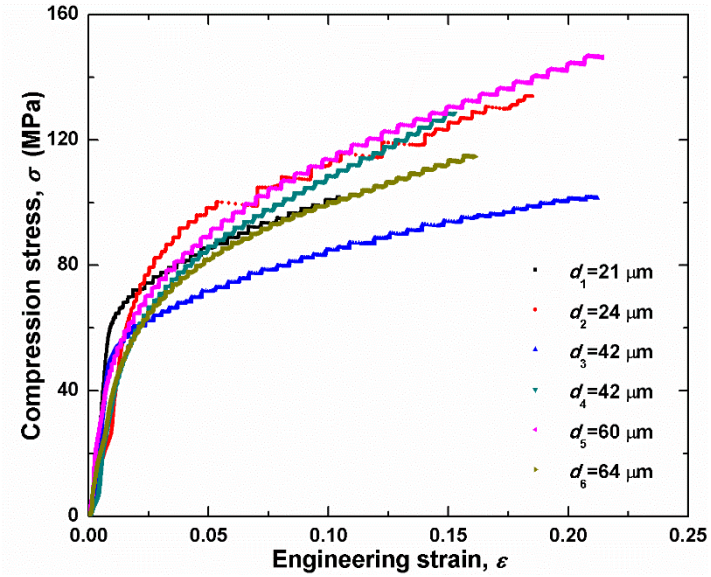

Fig. S3. Compression stress – engineering strain curves for Al micro-pillars of varying diameters

S3. Correction for the effect of pillar taper angle

Because of the existence of taper in PFIB Al pillars, the pillar top cross-sectional area is the smallest, and thus the calculated stress based on it is higher than the actual stress experienced by the pillar. To correct for the effect of the taper angle, a continuum plasticity finite element analysis (FEA) was carried out using the commercial ABAQUS FEA package. The Young's modulus and Poisson's ratio of Al were taken respectively as its bulk values, E = 70 GPa and ν = 0.33. The pillar geometry was built to be the same as the Al pillar shown in Fig. S1(b), namely, a top diameter of 24 μm, a height of 33 μm, and a taper angle of 9°. As the true mechanical response of the Al micro-pillar is unknown, the input material behavior to the FEA was taken as the measured plastic response of the 3.00 mm diameter Al rod specimen, shown as $\lambda = 1$ in Fig. S4(a). Then this measured input flow stress was scaled down by a factor of 2 and scaled up by a factor of 5, shown respectively as $\lambda = 0.5$ and $\lambda = 5$ in Fig. S4(a), to capture the effect of possible variation in the pillar response, which is unknown. Figure S4(b) displays the FEA outputs. The average stress at the top of the pillar (σ_{top}) and the average stress of the entire pillar (σ_{avg}) are obtained to represent the measured compression stress from experiment and the true average stress experienced by the pillar. With scaling factors of λ = 0.5, 1.0, and 5.0, the FEA generated σ_{avg} curves show good agreement with the corresponding input stress – strain curves, while the σ_{top} values are significantly higher at the same engineering strain. The ratio of σ_{top} and σ_{avg} is plotted as a function of the engineering strain, and shown in Fig. S4(c). As engineering strain varies from 0 to 15%, the value of $\sigma_{top}/\sigma_{avg}$ varies from 1.46 to 1.32 — a relative difference of 10%. The variation of $\sigma_{top}/\sigma_{avg}$ ratio with engineering strain exhibits a similar trend even when λ varies significantly, from 0.5 to 5.0. The values of $\sigma_{top}/\sigma_{avg}$ at the engineering strain of 10% are respectively 1.349, 1.352, and 1.359 at λ values of 0.5, 1.0, and 5.0, with an average of 1.353.

Based on the FEA results above, we divide the experimentally obtained pillar compression stresses as shown in Fig. S3 by 1.353 to arrive at the true pillar compression stress.

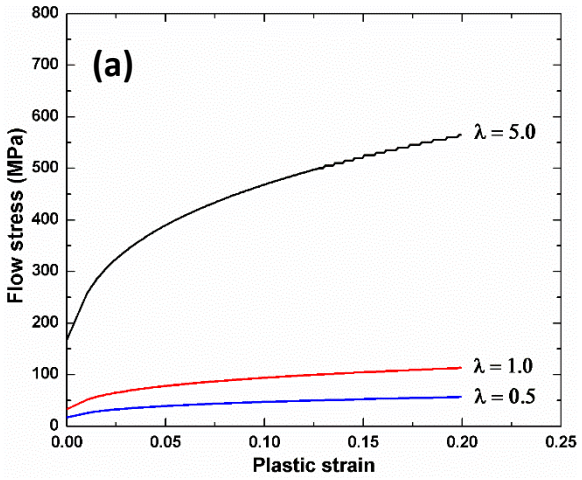

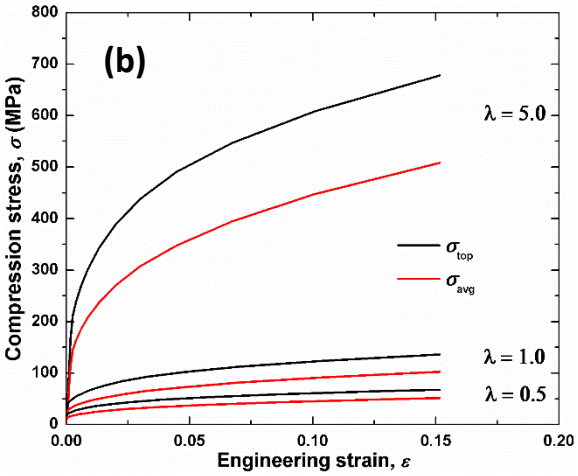

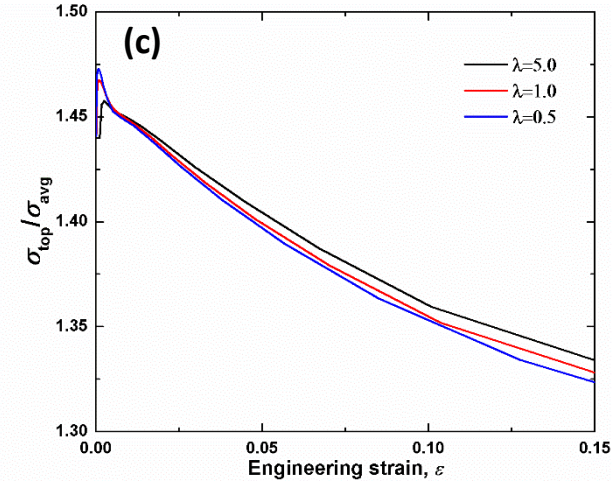

Fig. S4. FEA of compression of tapered pillars: (a) FEA input flow stress vs. plastic strain; (b) FEA outputs, as explained in the text; (c) ratio of $\sigma_{top}/\sigma_{avg}$.